



Observation of stratosphere–troposphere exchange during a pre-monsoon thunderstorm activity over Kochi, India

S. P. Sujithlal¹ · K. Satheesan^{1,2} · Ajil Kottayil² · K. Mohanakumar²

Received: 7 April 2021 / Accepted: 24 April 2022 / Published online: 24 May 2022
© The Author(s), under exclusive licence to Springer-Verlag GmbH Austria, part of Springer Nature 2022

Abstract

A severe thunderstorm developed on May 18, 2017 over the Kochi (10.03°N, 76.33°E), a coastal region located in the south-west Peninsular India, with overshooting tops as high as 16 km. Observations made using stratosphere troposphere (ST) radar located at Kochi during May 17–19, 2017 show that strong convection reached the tropopause height during this event, and considerable mixing has happened. This paper describes the exchange between the stratosphere and troposphere during this thunderstorm event, a few days prior to the onset of Indian Summer Monsoon. The air near the vicinity of the tropopause was characterised by notably high concentrations of humidity and CO. A tongue of air with stratospheric characteristics lay below the tropopause, showing that extensive stratosphere–troposphere exchange had occurred. The effects of such a mechanism on atmospheric budgets of trace species in the stratosphere may alter the lower stratosphere's chemistry. Detailed estimates of the fluxes are also presented in the paper.

1 Introduction

Understanding the dynamic coupling between the stratosphere and troposphere and the exchange of water vapor, momentum, energy, and trace gases between these two layers have much significance in climate studies (Dessler et al. 2013; Solomon et al. 2010; Murgatroyd and O'Neill 1980). Recent studies indicate that stratospheric water vapor and its variability play an important role in climate (Wang et al. 2017; Banerjee et al. 2019; Sherwood et al. 2003). Increase in stratospheric water vapor cool the stratosphere but warms the troposphere and vice versa. The positive trend in global temperature during 1980–2000 was strongly related to the elevated water vapor concentration in the stratosphere. A significant drop in the stratospheric water vapor after the year 2000 retarded the global temperature's positive trend (Solomon et al. 2010). As a result, paying more attention

to water vapour variability and the transport mechanisms involved is necessary.

The troposphere to stratosphere air transport mostly occurs across tropical tropopause (Brewer 1949). Holton et al. (1995) showed that such transports occur along the region just above the tropopause (~ 100 hPa) and tropopause temperature control the amount of water vapour that enters the stratosphere (Fueglistaler et al. 2009; Jain et al. 2006). Water vapour variability in the upper troposphere and lower stratosphere (UTLS) is closely related to the dynamics and thermodynamics of deep convective systems. Riehl and Malkus (1958) introduced the concept of penetration of cumulus convection into the stratosphere and the possibility of mass flux transport across the tropopause. Convective penetration above the Hadley cell (~ 14 km) is very rare, and the air injected above this layer subsequently participates in vertical ascent into the stratosphere (Folkins et al. 1999). On the other hand, Stratosphere to Troposphere Transport (STT) is a common phenomenon in the mid-latitudes which influences tropospheric O₃ levels (Collins et al. 2003). Descent through the dry air stream of mid-latitude cyclones is the primary mechanism for transporting stratospheric O₃ to the mid- and lower troposphere (Johnson and Viezee 1981; Cooper et al. 2001). In the tropics also, STT is associated with convective processes (Das 2009; Cairo et al. 2008), and it influences tropospheric O₃ levels.

Responsible Editor: Rubin Jiang.

✉ S. P. Sujithlal
spsujithlal@gmail.com

¹ Department of Atmospheric Sciences, Cochin University of Science And Technology, Kochi, India

² Advanced Centre for Atmospheric Radar Research, Cochin University of Science And Technology, Kochi, India

In this study, we focus on the stratosphere-troposphere exchange (STE) processes occurring through the tropical tropopause layer (TTL), the region between zero net radiative heating level to the highest level where convection reach. It acts as a gateway to the stratosphere from the troposphere (Fueglistaler et al. 2009) and plays an important role in trace substances' dynamics and chemistry. Quantification of trace gases and mass flux through this region is a challenging task but is essential for understanding the chemistry and dynamics of STE. The different small-scale processes associated with TTL are also significant in STE. They include enhanced turbulence (Fujiwara et al. 2003), shear instabilities (strong vertical shear in horizontal wind leads to Kelvin Helmholtz instability), and weakening of tropopause associated with convective systems (Kumar 2006; Das 2009).

The present study reports the STE processes during deep convection using a stratosphere–troposphere radar (ST radar) operating at Kochi (10.03°N, 76.33°E). A detailed study of the modification of tropopause structure and its dynamics is complicated using satellite observations alone, due to the lower spatio-temporal resolution. On the other hand, clear-air VHF radars can continuously monitor the tropopause structure with high vertical resolution and can also used to study STE process efficiently (Gage and Green 1982; Hocking et al. 2007; Das 2009; Das et al. 2016b; Narayana Rao et al. 2008). Hocking et al. (2007) studied the detection of stratospheric air and ozone intrusion into the stratosphere using a VHF radar. Hocking et al. (2007) have shown that enhanced radar backscattering power in the middle troposphere attributed to enhanced tropospheric ozone and stratospheric dry air so radar can be used as the proxy of the ozone intrusion and mixing of air. We adopted the same methodology to study STE process using ST radar. The current findings will help scientific community to understand better how deep convection affects the exchange of minor constituents between the troposphere and the stratosphere using ST radar.

2 Data and methodology

2.1 Radar observations

ST radar (205 MHz) at the Cochin University of Science And Technology (CUSAT) is an active phased array radar with 619 three-element Yagi-Uda antennas, arranged in an equilateral triangular grid. It covers 572 m² with an effective aperture area of 536 m² and has a power aperture product of 1.6×10^8 Wm² (Mohanakumar et al. 2017). ST radar provides three-dimensional wind profile data with an altitude range of 315 m to 20 km. The radar can be operated under two modes, the Doppler beam swinging (DBS) mode and the spaced antenna method (SAM). Here we use the DBS

method to derive wind profiles. The radar beam can be tilted at angles of 0°–30° in off-zenith direction and 0°–360° in azimuth direction at every 1° interval, thus capturing the three-dimensional picture of atmospheric features. The specifications of 205 MHz ST radar have been shown in Table 1.

The highest vertical resolution that can be obtained from this radar is 45 m. The radar wind profiles are validated against radiosonde with an accuracy of 2 m s⁻¹ for zonal and meridional wind profiles (Kottayil et al. 2016). The radar has been used for studying tropospheric features (Kottayil et al. 2018, 2019).

We used profiles of signal-to-noise ratio (SNR), Doppler width, and zonal and meridional winds with a vertical resolution of 180 m for May 17–19, 2017, and temporal resolution of 6 min. Continuous observations were made during this period. Radar wind measurements in coded modes of operation at a baud rate of and 1.2 μs have been used thus having a vertical resolution of 180 m. We have applied a quality control on radar data by inspecting the spectral moments. We checked the line of sight winds from symmetric beams, and whenever the Doppler in those beams were showing large differences in their amplitude, they were excluded. Further, wind profiles, which were not showing temporal continuity in the horizontal wind field, were also removed. The spectral width from the ST radar contains information on the turbulence intensity of the atmosphere. Here, we make use of spectral width to understand the turbulence during convection. The spectral width observed

Table 1 The specifications of 205 MHz ST radar

Parameters	Value
Frequency	205 MHz
Bandwidth	5 MHz
Type of system	Active phased array with TRM
Antenna element	Three-element Yagi-Uda antenna
Height coverage	315 m–20 km
Range gates	1024 (programmable)
Modes of operation	DBS
Height resolution	~ 180 m
One-way half-power beam width	~ 3.2°
Off-zenith angle	0°
Pulse width	0.3–76.8 μs
Baud	0.3–4.8 μs in steps of 0.3 μs
Pulse repetition frequency (PRF)	620 Hz
TRM transmit peak power	500 W
Radar system sensitivity	–165 dBm
Dynamic range	70 dB (min)
Type of receiver	Direct bandwidth sampling
Type of signal processor	FFT-based frequency domain
Gain of whole array	35 dBi
Receiver noise figure	< 3 dB

includes turbulence as well as non-turbulent effects like beam, shear, and wave broadening (Hocking 1985; Murphy et al. 1994; Nastrom and Eaton 1997)). Based on the equations from the literature (Nastrom and Eaton 1997; Hocking 1985), we have corrected the observed spectral width.

2.2 Reanalysis data

Modern-Era Retrospective Analysis for Research and Applications (MERRA–2) reanalysis data have also been used. MERRA–2 reanalysis provides 3-hourly data at 42 pressure levels from the surface to 0.01 hPa. In MERRA-2, all fields are provided on the 0.625° longitude by 0.5° latitude grid, which includes assimilation of aerosol optical thickness from moderate resolution imaging spectro-radiometer (MODIS) and multi-angle imaging spectro-radiometer (MISR) satellite observations, providing, global data of chemical gases, aerosol species and meteorological parameters under all-weather conditions. In this study the profiles of vertical pressure velocity, mass fraction of cloud liquid water, the mass fraction of cloud ice water, relative humidity, and CO from May 17 to 19, 2017, have been used. Because the reanalysis product provides intensity of vertical air motion across a larger area, the magnitude of the reanalysis product and Radar observation may not be equivalent. Directional tendencies of reanalysis data shows that updrafts are well reproduced in reanalysis data, but not downdrafts (Uma et al. 2021). The MERRA-2 reanalysis is more comparable to observations over the Indian tropical region (Das et al. 2016a), and it is designed to understand chemical transport. CO has been commonly utilised as a tracer for chemical transport studies since it is a well-mixed chemical gas that is a consequence of industrial pollution and biomass burning. Surface emissions, atmospheric wind transport, and mixing are strongly connected to CO levels in the atmosphere, while chemical reactions and dry or wet removal have less effect. The MERRA-2 CO trends are generally consistent with observation data (AURA-MLS), but the magnitude is underestimated by roughly 10–20% in the deep tropics and by more than 50% in the extratropics. This could be attributable to inaccuracies in the MERRA-2 assimilation's assessment of biomass burning emission rates (Lau et al. 2017).

2.3 Satellite data

Globally-merged (60°S–60°N) 4 km pixel resolution IR brightness temperature data (equivalent blackbody temperature) is used for synoptic analysis, which is merged from the European, Japanese, and U.S. geostationary satellites over the period of record (GOES-8/9/10/11/ 12/13/14/15/16, METEOSAT-5/7/8/9/10, and GMS-5/MTSat-1R/2/Himawari-8). The spatial and temporal resolution of the data is 4 × 4 km and 30 min, respectively.

We also used the observations from the CALIOP instrument onboard satellite CALIPSO (Cloud-Aerosol Lidar and Infrared Pathfinder Satellite Observation) over Kochi on May 18 (Winker et al. 2007, 2009). During a day, CALIPSO performs approximately 15 orbits between 82°S and 82°N and has a repeat cycle of 16 days (Winker et al. 2010). It has optimized for aerosol and cloud profiling and linearly polarized laser pulses are transmitted at 532 nm and 1064 nm. In this study we have used CALIPSO 532 nm Total (Parallel + Perpendicular) attenuated backscatter (/km/sr). Profiles from CALIOP provide information on the vertical distributions of aerosols and clouds, cloud ice/water phase and a qualitative classification of aerosol size (Winker et al. 2007, 2009)). We used the data products available at <https://www-calipso.larc.nasa.gov>.

3 Results and discussion

3.1 Synoptic conditions

The high-resolution satellite observations have been used to understand the cloud cover over the radar location. Brightness temperature (T_b) less than 200 K shows the presence of deep convective clouds. The T_b observed over the Indian sub-continent on May 18, 2017 at 2130 hours local time (LT) is shown in the Fig. 1. The time series of T_b observed over the radar location is shown in Fig. 4. Convective clouds started forming at 1600 hours LT on 18 May 2017 (Fig. 4). Later, it intensified into a deep convective cloud system between 1800–2200 hours, which is evident from the low values (< 200 K) of T_b observed over Kochi. Such low level T_b indicates the probability of a cloud top reaching the tropopause level (Rao et al. 2004). The vertical profiles of

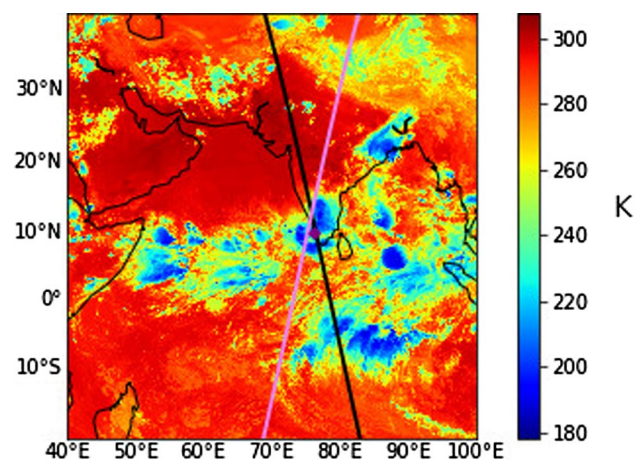


Fig. 1 Brightness temperature (K) at 2130 LST on May 18, 2017. The coloured lines indicate the tracks of the CALIPSO (daytime and nighttime) and star mark denotes radar location (10.03°N, 76.33°E)

the Total attenuated backscatter at 532 nm from CALIOP is shown in the Fig. 2a. The first one was taken on May 18, 2017, at 1400 hours LT, closer to the radar location (10.00°N, 76.44°E.) just before thunderstorm event and 2nd observation (Fig. 2b) has been taken after the deep convection on May 19, 2017 at 0100 hours LT in the same latitude (10.00°N, 75.33°E.). The back scattering profiles undoubtedly provide the evidence for deep convective cloud reaching up to 15–16 km.

3.2 Modification of tropopause

Figure 3 shows the height–time variation (10–20 km) of SNR deduced from the ST radar observations beginning from May 17–19, 2017. Continuous observations from ST radar were made on these days. The SNR is the function of refractive index gradient (C_n^2) of air. In turn, n is a function of temperature, humidity, pressure and electron density. In the lower and middle tropospheres, it is affected by temperature and humidity; in the mesosphere, it is affected by electron density (Fig. 4). But at UTLS it depends mainly on temperature due to the very low humidity in this region. Apart from the vertical shear of horizontal winds, sometimes the clouds in UTLS regions containing water vapor can also affect SNR. Partial reflection also contributes to the large SNR in the UTLS. Here a sharp increase in SNR around 16–17 km is noticed in Fig. 3.

The enhanced SNR arises due to the sharp gradient in n , due to gradient in temperature at 16–17 km. The SNR gradient at these heights is an accurate measurement of tropopause height (Gage and Green 1982; Gage et al. 1986; Satheesan and Krishna Murthy 2005). The cold point tropopause (CPT) height derived from the 205 MHz ST radar is in good agreement with that measured from radiosonde (Nithya et al. 2019). Hence, the sharp increase in SNR at tropopause levels is a proxy for cold point tropopause height. Cold-point tropopause (CPT) is estimated from ST radar and is superimposed (Fig. 3).

It can be seen that during deep convection, the enhancement in SNR occurs at a higher altitude than the normal conditions. The pattern change in SNR indicates modulation of tropopause over this location (Dhaka et al. 2002). The continuous collision of molecules due to deep convection weakens the tropopause since the strength of temperature gradient diminishes (Kumar 2006; Dhaka et al. 2002). The modified tropopause structure is different from the normal condition (Fig. 3) and can enhance stratosphere–troposphere exchange (Kumar 2006). The modified structure of tropopause and the turbulence present near to tropopause can be analysed using the Doppler width obtained from radar. Spectral width is directly proportional to the turbulence intensity. Strong turbulence was observed near the tropopause and lower altitudes during deep convective events. High

turbulence near the tropopause region enhances the possibility of exchange of constituents between the troposphere and stratosphere (Fig. 5).

The vertical velocity profiles during the three days obtained from the radar is shown in Fig. 6 which shows strong updrafts upto 16 km from 1600 to 2100 hours LT on May 18. The long persisting (~ 5 h) strong updrafts could be the reason for changes in the normal structure and stability of the tropopause, which is consistent with the results from Dhaka et al. (2002). Vertical velocity obtained from radar may sometimes be contaminated due to the presence of precipitation. Hence, we used the vertical pressure velocity from MERRA-2 also (figure not shown) and found similar structure as the radar estimated vertical velocities during this period. Tropical easterly jet (TEJ), a strong horizontal wind, is present in the upper troposphere during May 17–19 (Fig. 7a, b). The vertical shear (Fig. 7c) of horizontal wind induces instability in the TTL, which enhances the mixing processes near the tropopause and thus decreases the stability.

3.3 Observations of mass flux transport

Data from the MERRA-2 reanalysis is used to analyse the relative humidity, mass fraction of cloud ice water and cloud liquid water and is shown in Fig. 8. During deep convection, liquid clouds are formed between 5 and 10 km altitudes, and ice clouds are formed within 10–15 km (Fig. 8b, c). The relative humidity during this period attains saturation value (Fig. 8a), which indicates the vertical transport of humidity by deep convection, strong updrafts transporting water vapour from the troposphere to the lower stratosphere. Presence of cloud ice water between 200–100 hPa also shows this mass transport. We estimated the mass flux as a function of vertical velocity and density of air from MERRA-2 at radar location, which is given as $F_m = \rho V$. In the UTLS, mass flux enhances after the strong deep convection (Fig. 9). The peak in mass flux ($\sim 3 \text{ kg m}^{-2} \text{ s}^{-1}$; in the upward direction) is observed around 150–50 hPa. Vertically integrated mass flux shows that the over-shooting deep convection transports humid air from the troposphere to the UTLS region. The upward mass flux is inversely proportional to the stability of the tropopause. The water vapour intrusion from the upper troposphere to the lower stratosphere depends on the tropopause temperature. Tropospheric air could enter stratosphere where the tropopause temperature is the coldest (Newell and Gould-Stewart 1981). During deep convection, water vapor entered into the stratosphere undergoes freeze dry mechanism (Newell and Gould-Stewart 1981; Jain et al. 2006). The lowest tropopause temperature (obtained from MERRA-2) (~ 190 K) was found on May 17, 2017 (Fig. 9) when there is convection, but the mass

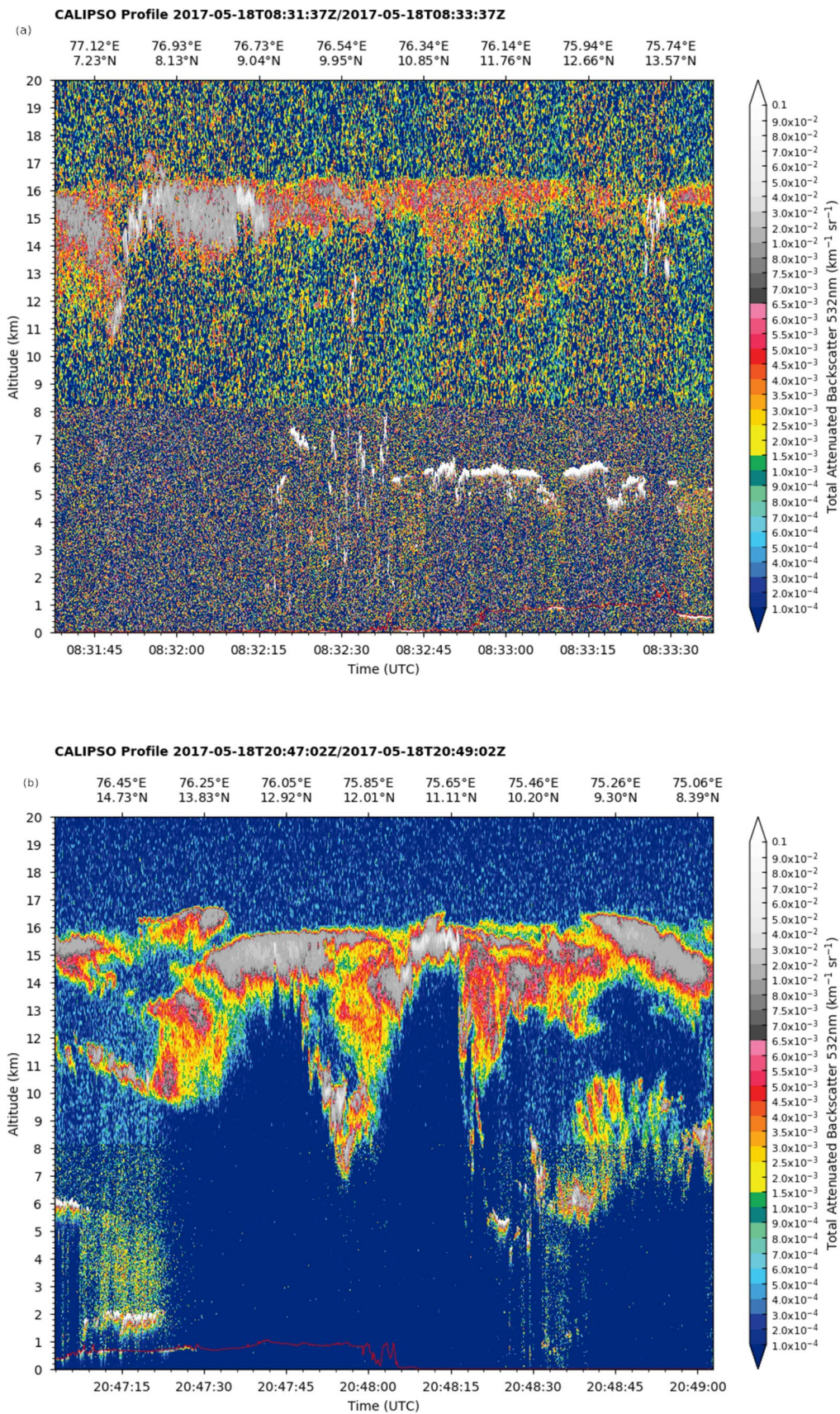


Fig. 2 Height-time images of CALIPSO 532 nm Total attenuated backscatter ($/\text{km}/\text{sr}$) for **a** daytime and **b** night time

Fig. 3 Height-time profiles of signal-to-noise ratio (dB). The black line drawn is the tropopause determined from the gradient of SNR, the start and end times of the convective event are marked by two vertical lines and the tongue shaped structure is marked as a dotted box

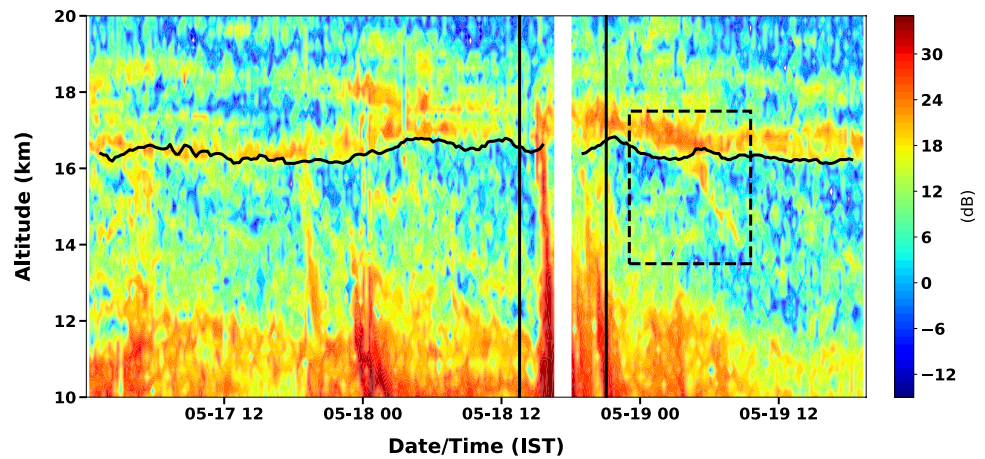


Fig. 4 Time series of brightness temperature during during May 16–21, 2017. The start and end times of the convective event are marked by two vertical lines

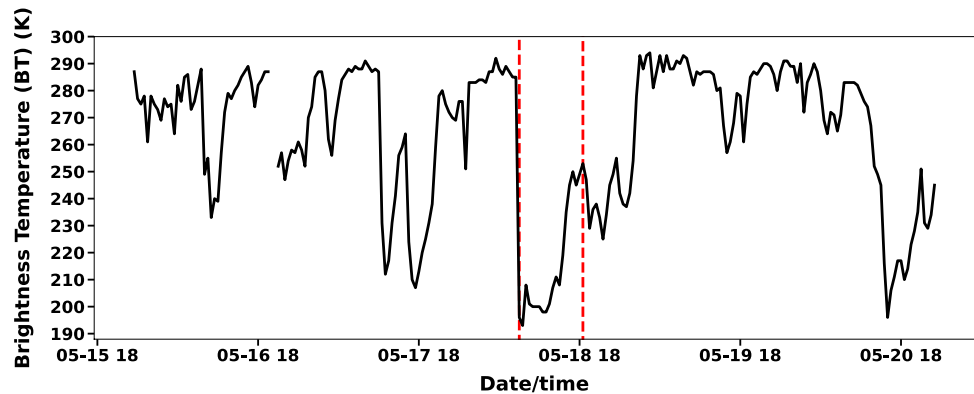
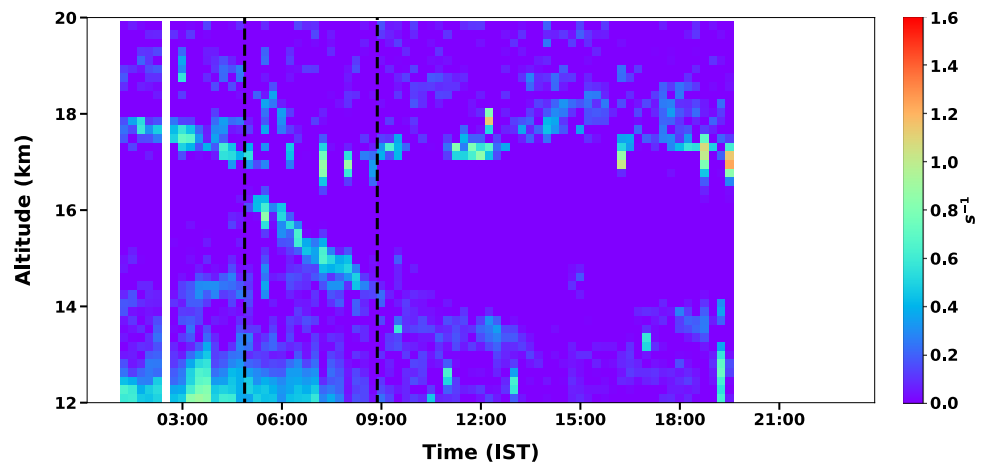


Fig. 5 Doppler width (s^{-1}) observed after deep convection event on May 19, 2017. The start and end times of the stratospheric intrusion are marked by two vertical lines



transport however is negligible. During the strong convection on May 18, 2017 tropopause temperature remains warmer (~ 192 K) than the previous day, and mass flux transport was evident. A recent study by Wu et al. (2020) suggested that convective processes are responsible for transport of tracers upto 200–300 hPa whereas vertical eddy flux dominates in the UTLS. The major results of

our study is in agreement with Wu et al. (2020). Strong upward motion persists upto the level of 14–15 km and above that, the vertical shear (Fig. 7c) of the horizontal wind induces instability and eddies. Thus, the stability of tropopause, vertical wind shear, and smaller scale turbulence play major roles in mass exchange rather than the tropopause temperature only.

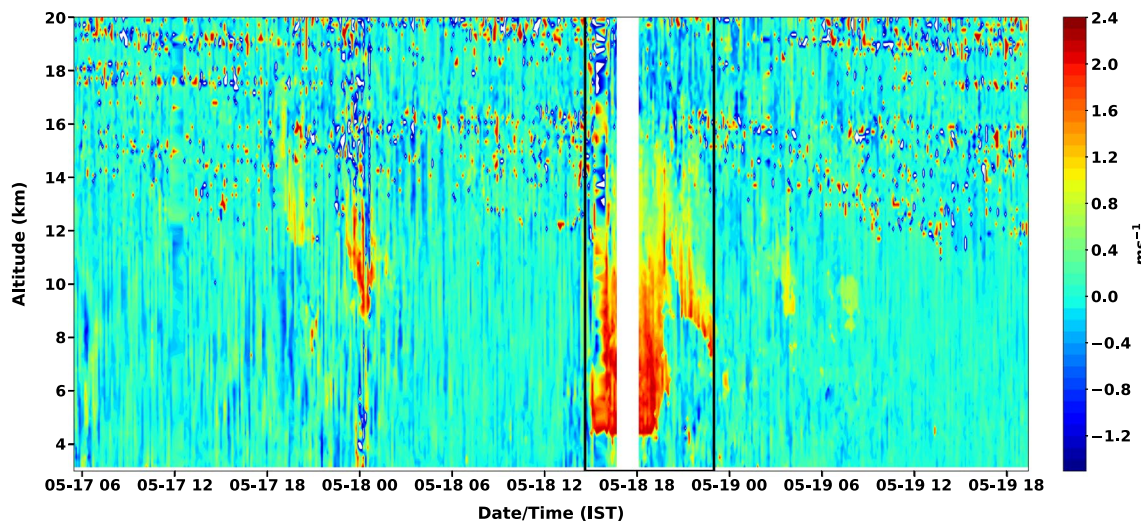
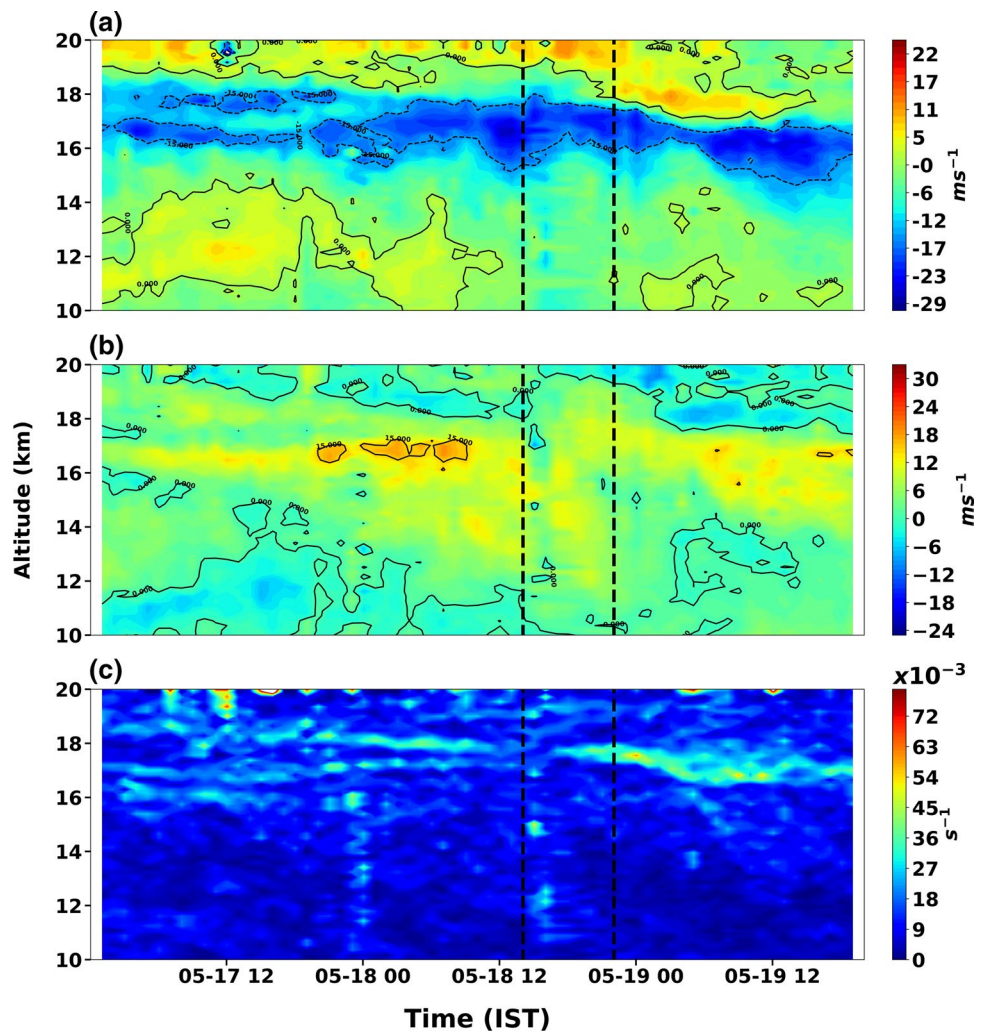


Fig. 6 Height-time profiles of vertical velocity (m s^{-1}) during May 17–20, 2017, The start and end times of the convective event are marked by two vertical lines

Fig. 7 Height - time intensity of hourly **a** zonal wind (m s^{-1}), **b** meridional wind (m s^{-1}) and **c** wind shear (s^{-1}) during May 17–19, 2017. The start and end times of the convective event are marked by two vertical lines



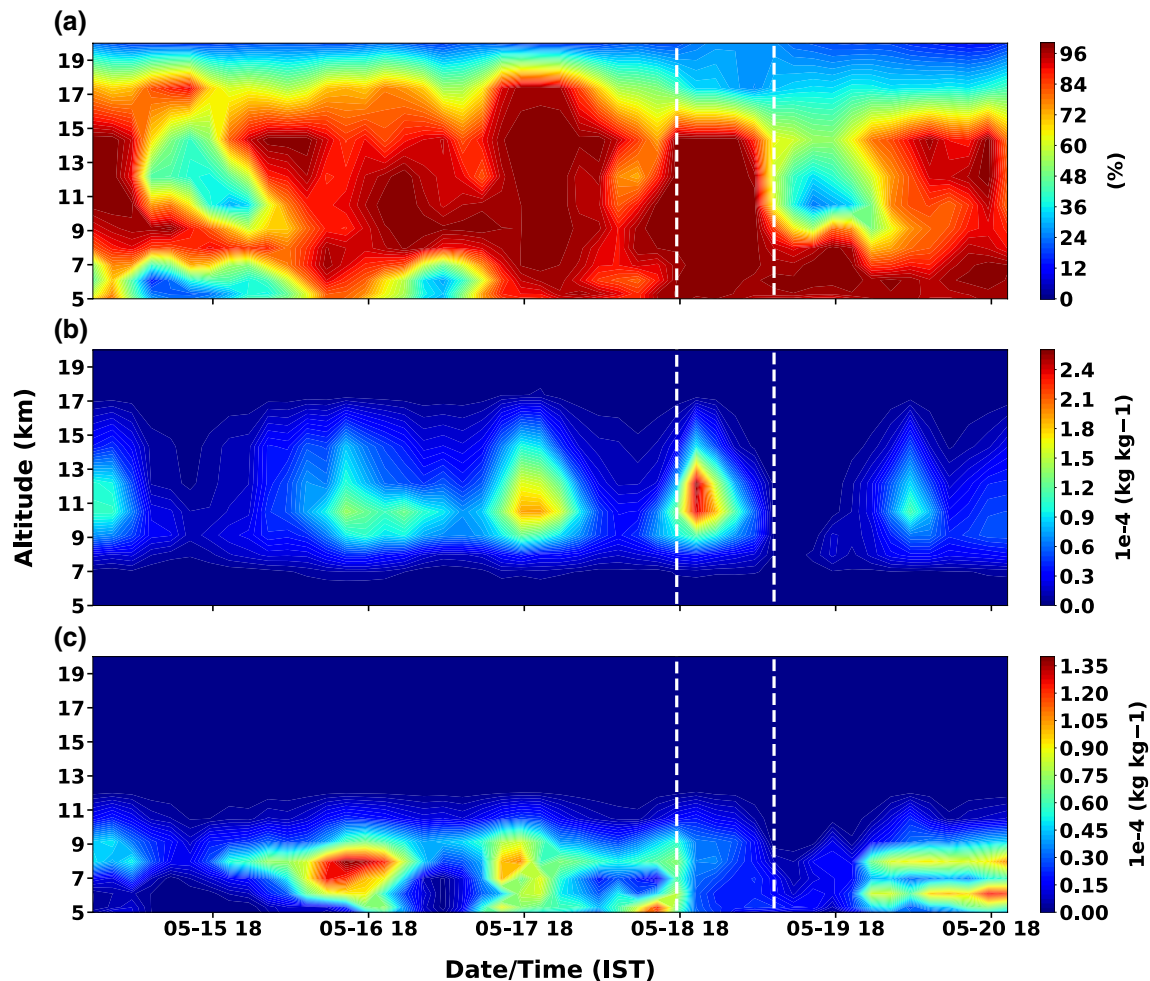


Fig. 8 Height-time intensity of **a** relative humidity unit in %, **b** mass fraction of cloud ice water (kg kg^{-1}) and **c** mass fraction of cloud liquid water (kg kg^{-1}) during May 15–21 2017. The start and end times of the convective event are marked by two vertical lines.

3.4 Carbon monoxide as a tracer

Carbon monoxide (CO) observations in the stratosphere is usually used to understand the dynamical processes since the photo-chemical lifetime of CO is longer than the time scale of many of the dynamical problems of interest. Due to the low mixing ratio in the lower stratosphere, CO can act as an important tracer of STE during intense convective activity (Ricaud et al. 2007). CO is mostly concentrated in the lower troposphere than the stratosphere and is of anthropogenic origin. As a result, any elevated concentration of CO in the stratosphere can be directly related to the STE processes. The lifetime of CO in the stratosphere is high compared to troposphere (Hoor et al. 2004; Schoeberl et al. 2006; Pfister et al. 2004). We analysed the CO profiles from MERRA-2 during the event (Fig. 10). MERRA-2 data are in general agreement with satellite observations, but the magnitude is underestimated by 10–20% in tropics, it may be due to uncertainties of biomass emission rate used in MERRA-2

assimilation system. Throughout the study period, CO shows higher values in the lower troposphere, whereas on May 19, 2017, the entire atmospheric column from 0 to 18 km has elevated CO concentration, which again proves STE and is seen to peak (80 ppb) around 18 km. The increased volume mixing ratio of CO is observed when the tropopause structure is disrupted. It is clear that CO is carried vertically from surface to 15 km by high vertical advection and further carried by turbulence and eddies induced by TEJ. The high lifetime of CO in the stratosphere, in conjunction with its anthropogenic origin makes the studies of CO more significant. Its chemical as well as radiative effect in the stratosphere requires further studies.

3.5 Indication of stratospheric air intrusion into the upper troposphere

Though vertical velocity does not show significant changes after the deep convective activity, unusual observations

Fig. 9 Time series of vertically integrated mass flux (150–50 hPa) (black line) and tropopause temperature (red line) during May 17–19, 2017. The start and end times of the convective event are marked by two vertical lines

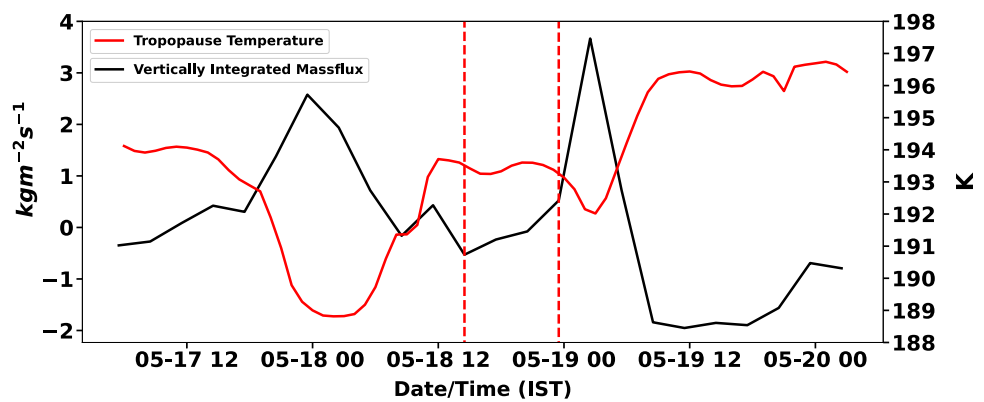
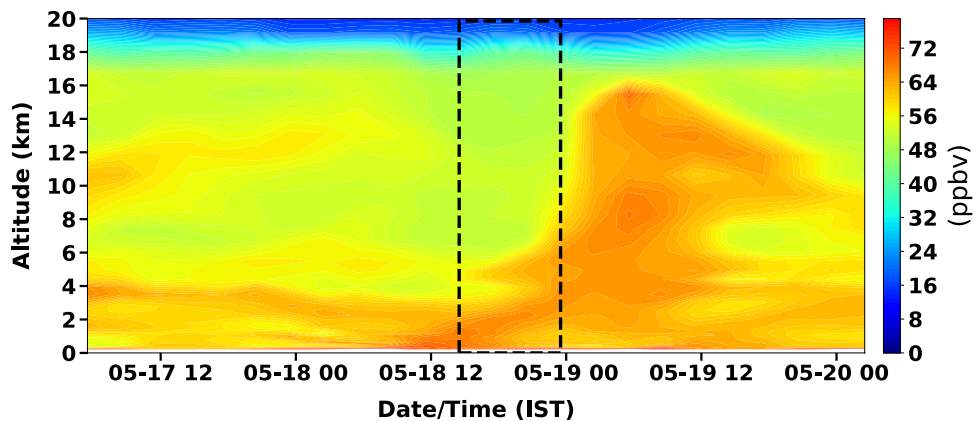


Fig. 10 Height-time intensity of CO (unit in ppbv) during May 17–19, 2017. The start and end times of the convective event are marked by two vertical lines



have seen in SNR and in the Doppler width in the UTLS region from 0100 to 0400 Hrs LT on May 19, 2017. A tongue-shaped SNR gradient is observed in the UTLS region (Fig. 3) which probably indicates the downward transport of stable dry stratospheric air through the tropopause. The relative humidity during the vertical mass transport was higher, but immediately after the event, it is reduced to less than 30% between the altitude levels 10–15 km (Fig. 8a). The mass fraction of cloud liquid and ice water profile shows a substantial reduction immediately after the mass flux transport. It indicates the possibility of dry air intrusion from the stratosphere to the upper troposphere. An enhanced turbulent activity is observed in the UTLS region, and a tongue-shaped SNR could indicate a downward transport of stable dry stratospheric air through the tropopause (Fig. 5). Doppler width from the radar is a proxy of turbulence activity in the troposphere, which shows enhancement after deep convective event. A sudden change in the zonal and meridional wind pattern is also noticed during the observation of the tongue-shaped structure of SNR, which further supports the possibility of dry air intrusion from the stratosphere to the troposphere (Fig. 7).

4 Conclusions

In this study, we analyzed the stratosphere-troposphere exchange observed after an intense deep thunderstorm event on May 18, 2017 over Kochi. Observations from a ST radar taken during May 17–19, 2017, have been utilized to study the STE processes with supplementary satellite observations and reanalysis data to study the stratosphere-troposphere exchange.

The vertically integrated mass flux shows that the overshooting deep convection transports humid air from the lower troposphere to the UTLS region. The peak in mass flux ($\sim 3 \text{ kgm}^2 \text{ s}^{-1}$; in the upward direction) is observed around 150–50 hPa during the event. The higher concentration of CO obtained from MERRA-2 further confirms the transport. We show that the upper-tropospheric turbulence and wind shear can affect the tropopause, which can eventually aid in the vertical transport of mass from the tropopause to the lower stratosphere and vice-versa. From the observation of SNR and corrected Doppler width; a tongue of air with stratospheric characteristics lay below the tropopause, showing that extensive stratosphere–troposphere exchange had occurred.

Acknowledgements The authors would like to thank the Science Engineering Research Board (SERB), Department of Science and Technology (DST), Government of India, for the support in establishing the 205 MHz ST radar at ACARR, CUSAT. The financial support provided by the Ministry of Earth Sciences (MoES), Government of India for the sustenance of the ST radar Facility is greatly acknowledged.

Data Availability The data sets (both radars and reanalyses) analysed during the current study are available from the corresponding author on reasonable request. Reanalysis data (MERRA-2) is publicly available: https://gmao.gsfc.nasa.gov/reanalysis/MERRA-2/data_access/.

References

- Banerjee A, Chiodo G, Previdi M, Ponater M, Conley AJ, Polvani LM (2019) Stratospheric water vapor: an important climate feedback. *Clim Dyn* 53(3–4):1697–1710. <https://doi.org/10.1007/s00382-019-04721-4>
- Brewer AW (1949) Evidence for a world circulation provided by the measurements of helium and water vapour distribution in the stratosphere. *Q J R Meteorol Soc* 75(326):351–363. <https://doi.org/10.1002/qj.49707532603>
- Cairo F, Buontempo C, MacKenzie AR, Schiller C, Volk CM, Adriani A, Mitev V, Matthey R, Di Donfrancesco G, Oulanovsky A, Ravegnani F, Yushkov V, Snels M, Cagnazzo C, Stefanutti L (2008) Morphology of the tropopause layer and lower stratosphere above a tropical cyclone: a case study on cyclone Davina (1999). *Atmos Chem Phys* 8(13):3411–3426. <https://doi.org/10.5194/acp-8-3411-2008>. <https://acp.copernicus.org/articles/8/3411/2008/>
- Collins WJ, Derwent RG, Garnier B, Johnson CE, Sanderson MG, Stevenson DS (2003) Effect of stratosphere-troposphere exchange on the future tropospheric ozone trend. *J Geophys Res Atmos* 108(D12). <https://doi.org/10.1029/2002JD002617>. <https://agupubs.onlinelibrary.wiley.com/doi/abs/10.1029/2002JD002617>
- Cooper OR, Moody JL, Parrish DD, Trainer M, Ryerson TB, Holloway JS, Hübler G, Fehsenfeld FC, Oltmans SJ, Evans MJ (2001) Trace gas signatures of the airstreams within north Atlantic cyclones: Case studies from the north Atlantic regional experiment (nare '97) aircraft intensive. *J Geophys Res Atmos* 106(D6):5437–5456. <https://doi.org/10.1029/2000JD900574>, <https://agupubs.onlinelibrary.wiley.com/doi/abs/10.1029/2000JD900574>
- Das SS (2009) A new perspective on mst radar observations of stratospheric intrusions into-troposphere associated with tropical cyclone. *Geophys Res Lett* 36(15). <https://doi.org/10.1029/2009GL039184>
- Das SS, Uma KN, Bineesha VN, Suneeth KV, Ramkumar G (2016) Four-decadal climatological intercomparison of rocketsonde and radiosonde with different reanalysis data: results from thumba equatorial station. *Q J R Meteorol Soc* 142(694):91–101. <https://doi.org/10.1002/qj.2632>. <https://rmets.onlinelibrary.wiley.com/doi/abs/10.1002/qj.2632>
- Das SS, Venkat Ratnam M, Uma KN, Patra AK, Subrahmanyam KV, Girach IA, Suneeth KV, Kumar KK, Ramkumar G (2016) Stratospheric intrusion into the troposphere during the tropical cyclone Nilam (2012). *Q J R Meteorol Soc* 142(698):2168–2179. <https://doi.org/10.1002/qj.2810>
- Dessler AE, Schoeberl MR, Wang T, Davis SM, Rosenlof KH (2013) Stratospheric water vapor feedback. *Proc Natl Acad Sci* 110(45):18087–18091. <https://doi.org/10.1073/pnas.1310344110>
- Dhaka SK, Choudhary RK, Malik S, Shibagaki Y, Yamanaka MD, Fukao S (2002) Observable signatures of a convectively generated wave field over the tropics using Indian MST radar at Gadanki (13.5°N, 79.2°E). *Geophys Res Res* 29(18):1872. <https://doi.org/10.1029/2002GL014745>
- Folkens I, Loewenstein M, Podolske J, Oltmans SJ, Proffitt M (1999) A barrier to vertical mixing at 14 km in the tropics: evidence from ozonesondes and aircraft measurements. *J Geophys Res Atmos* 104(D18):22095–22102. <https://doi.org/10.1029/1999JD900404>
- Fueglistaler S, Dessler AE, Dunkerton TJ, Folkens I, Fu Q, Mote PW (2009) Tropical tropopause layer. *Rev Geophys* 47(1). <https://doi.org/10.1029/2008RG000267>
- Fujiwara M, Xie SP, Shiotani M, Hashizume H, Hasebe F, Vomel H, Oltmans SJ, Watanabe T (2003) Upper-tropospheric inversion and easterly jet in the tropics. *J Geophys Res Atmos* 108(D24). <https://doi.org/10.1029/2003JD003928>
- Gage KS, Ecklund WL, Riddle AC, Balsley BB (1986) Objective tropopause height determination using use-resolution vhf radar observations. *J Atmos Ocean Technol* 3(2):248–254. [https://doi.org/10.1175/1520-0426\(1986\)003<0248:OTHUU>2.0.CO;2](https://doi.org/10.1175/1520-0426(1986)003<0248:OTHUU>2.0.CO;2)
- Gage KS, Green JL (1982) An objective method for the determination of tropopause height from vhf radar observations. *J Appl Meteorol* 21(8):1150–1154. [https://doi.org/10.1175/1520-0450\(1982\)021<1150:AOMFTD>2.0.CO;2](https://doi.org/10.1175/1520-0450(1982)021<1150:AOMFTD>2.0.CO;2)
- Hocking WK (1985) Measurement of turbulent energy dissipation rates in the middle atmosphere by radar techniques: a review. *Radio Sci* 20:1403–1422. <https://doi.org/10.1029/RS020i006p01403>
- Hocking WK, Carey-Smith T, Tarasick DW, Argall PS, Strong K, Rochon Y, Zawadzki I, Taylor PA (2007) Detection of stratospheric ozone intrusions by windprofiler radars. *Nature* 450(7167):281–284. <https://doi.org/10.1038/nature06312>
- Holton JR, Haynes PH, McIntyre ME, Douglass AR, Rood RB, Pfister L (1995) Stratosphere-troposphere exchange. *Rev Geophys* 33(4):403–439. <https://doi.org/10.1029/95RG02097>
- Hoor P, Gurk C, Brunner D, Hegglin MI, Wernli H, Fischer H (2004) Seasonality and extent of extratropical tst derived from in-situ co measurements during spurt. *Atmos Chem Phys* 4(5):1427–1442. <https://doi.org/10.5194/acp-4-1427-2004>, <https://www.atmos-chem-phys.net/4/1427/2004/>
- Jain AR, Das SS, Mandal TK, Mitra AP (2006) Observations of extremely low tropopause temperature over the Indian tropical region during monsoon and postmonsoon months: Possible implications. *J Geophys Res Atmos*. <https://doi.org/10.1029/2005JD005850>
- Johnson WB, Viezee W (1981) Stratospheric ozone in the lower troposphere—I. presentation and interpretation of aircraft measurements. *Atmos Environ* (1967) 15(7):1309–1323. [https://doi.org/10.1016/0004-6981\(81\)90325-5](https://doi.org/10.1016/0004-6981(81)90325-5)
- Kottayil A, Mohanakumar K, Samson T, Rebello R, Manoj MG, Varadarajan R, Santosh KR, Mohanan P, Vasudevan K (2016) Validation of 205 MHz wind profiler radar located at cochin, India, using radiosonde wind measurements. *Radio Sci* 51(3):106–117. <https://doi.org/10.1002/2015RS005836>
- Kottayil A, Satheesan K, Mohankumar K, Chandran S, Samson T (2018) An investigation into the characteristics of inertia gravity waves in the upper troposphere/lower stratosphere using a 205 mhz wind profiling radar. *Remote Sens Lett* 9(3):284–293. <https://doi.org/10.1080/2150704X.2017.1418991>
- Kottayil A, Xavier P, Satheesan K, Mohanakumar K, Rakesh V (2019) Vertical structure and evolution of monsoon circulation as observed by 205-MHz wind profiler radar. *Meteorol Atmos Phys*. <https://doi.org/10.1007/s00703-019-00695-4>
- Kumar KK (2006) Vhf radar observations of convectively generated gravity waves: Some new insights. *Geophys Res Lett*. <https://doi.org/10.1029/2005GL024109>
- Lau WKM, Yuan C, Li Z (2017) Origin, maintenance and variability of the asian tropopause aerosol layer (ATAL): the roles of monsoon dynamics. *AGU Fall Meeting Abstr* 2017:A12E-02

- Mohanakumar K, Kottayil A, Anandan VK, Samson T, Thomas L, Satheesan K, Rebello R, Manoj MG, Varadarajan R, Santosh KR, Mohanan P, Vasudevan K (2017) Technical details of a novel wind profiler radar at 205 MHz. *J Atmos Oceanic Technol* 34(12):2659–2671. <https://doi.org/10.1175/JTECH-D-17-0051.1>
- Murgatroyd RJ, O'Neill A (1980) Interaction between the troposphere and stratosphere. *Philos Trans R Soc Lond Ser A Math Phys Sci* 296(1418):87–102. <http://www.jstor.org/stable/36437>
- Murphy DJ, Hocking WK, Fritts DC (1994) An assessment of the effect of gravity waves on the width of radar Doppler spectra. *J Atmos Terr Phys* 56:17–29. [https://doi.org/10.1016/0021-9169\(94\)90172-4](https://doi.org/10.1016/0021-9169(94)90172-4)
- Narayana Rao T, Uma KN, Narayana Rao D, Fukao S (2008) Understanding the transportation process of tropospheric air entering the stratosphere from direct vertical air motion measurements over Gadanki and Kototabang. *Geophys Res Lett.* <https://doi.org/10.1029/2008GL034220>
- Nastrom GD, Eaton FD (1997) Turbulence eddy dissipation rates from radar observations at 5–20 km at White Sands Missile Range, New Mexico. *J Geophys Res Atmos* 102:19. <https://doi.org/10.1029/97JD01262>
- Newell RE, Gould-Stewart S (1981) A stratospheric fountain? *J Atmos Sci* 38(12):2789–2796. [https://doi.org/10.1175/1520-0469\(1981\)038<2789:ASF>2.0.CO;2](https://doi.org/10.1175/1520-0469(1981)038<2789:ASF>2.0.CO;2)
- Nithya K, Kottayil A, Mohanakumar K (2019) Determining the tropopause height from 205 MHz stratosphere troposphere wind profiler radar and study the factors affecting its variability during monsoon. *J Atmos Solar Terr Phys* 182:79–84
- Pfister G, Pétron G, Emmons LK, Gille JC, Edwards DP, Lamarque JF, Attie JL, Granier C, Novelli PC (2004) Evaluation of co simulations and the analysis of the co budget for Europe. *J Geophys Res Atmos.* <https://doi.org/10.1029/2004JD004691>
- Rao KG, Desbois M, Roca R, Nakamura K (2004) Upper tropospheric drying and the “transition to break” in the Indian summer monsoon during 1999. *Geophys Res Lett.* <https://doi.org/10.1029/2003GL018269>
- Ricaud P, Barret B, Attié JL, Motte E, Le Flochmoën E, Teyssèdre H, Peuch VH, Livesey N, Lambert A, Pommereau JP (2007) Impact of land convection on troposphere-stratosphere exchange in the tropics. *Atmos Chem Phys* 7(21):5639–5657. <https://doi.org/10.5194/acp-7-5639-2007>
- Riehl H, Malkus JS (1958) On the heat balance in the equatorial trough zone. *Geophysica* 6:503–538
- Satheesan K, Krishna Murthy BV (2005) A study of tropical tropopause using mst radar. *Ann Geophys* 23(7):2441–2448. <https://doi.org/10.5194/angeo-23-2441-2005>
- Schoeberl MR, Duncan BN, Douglass AR, Waters J, Livesey N, Read W, Filipiak M (2006) The carbon monoxide tape recorder. *Geophys Res Lett.* <https://doi.org/10.1029/2006GL026178>
- Sherwood SC, Horinouchi T, Zeleznik HA (2003) Convective impact on temperatures observed near the tropical tropopause. *J Atmos Sci* 60(15):1847–1856. [https://doi.org/10.1175/1520-0469\(2003\)060<1847:CIOTON>2.0.CO;2](https://doi.org/10.1175/1520-0469(2003)060<1847:CIOTON>2.0.CO;2), https://journals.ametsoc.org/view/journals/atcsc/60/15/1520-0469_2003_060_1847_cioton_2.0.co_2.xml
- Solomon S, Rosenlof KH, Portmann RW, Daniel JS, Davis SM, Sanford TJ, Plattner GK (2010) Contributions of stratospheric water vapor to decadal changes in the rate of global warming. *Science* 327(5970):1219–1223. <https://doi.org/10.1126/science.1182488>
- Uma KN, Das SS, Ratnam MV, Suneeth KV (2021) Assessment of vertical air motion among reanalyses and qualitative comparison with very-high-frequency radar measurements over two tropical stations. *Atmos Chem Phys* 21(3):2083–2103. <https://doi.org/10.5194/acp-21-2083-2021>. <https://acp.copernicus.org/articles/21/2083/2021/>
- Wang Y, Su H, Jiang JH, Livesey NJ, Santee ML, Froidevaux L, Read WG, Anderson J (2017) The linkage between stratospheric water vapor and surface temperature in an observation-constrained coupled general circulation model. *Clim Dyn* 48(7–8):2671–2683. <https://doi.org/10.1007/s00382-016-3231-3>
- Winker DM, Hunt WH, McGill MJ (2007) Initial performance assessment of caliop. *Geophys Res Lett.* <https://doi.org/10.1029/2007G1030135>
- Winker DM, Vaughan MA, Omar A, Hu Y, Powell KA, Liu Z, Hunt WH, Young SA (2009) Overview of the calipso mission and caliop data processing algorithms. *J Atmos Oceanic Technol* 26(11):2310–2323. <https://doi.org/10.1175/2009JTECHA1281.1>
- Winker DM, Pelon J, Coakley JJA, Ackerman SA, Charlson RJ, Colarco PR, Flamant P, Fu Q, Hoff RM, Kittaka C, Kubar TL, Le Treut H, McCormick MP, Mégie G, Poole L, Powell K, Trepte C, Vaughan MA, Wielicki BA (2010) The CALIPSO mission: a global 3D view of aerosols and clouds. *Bull Am Meteorol Soc* 91(9):1211–1230. <https://doi.org/10.1175/2010BAMS3009.1>
- Wu Y, Orbe C, Tilmes S, Abalos M, Wang X (2020) Fast transport pathways into the northern hemisphere upper troposphere and lower stratosphere during northern summer. *J Geophys Res Atmos* 125(3):e2019JD031552. <https://doi.org/10.1029/2019JD031552>

Publisher's Note Springer Nature remains neutral with regard to jurisdictional claims in published maps and institutional affiliations.